Regulation of Lipid-Droplet Alterations Upon Infection (Molecular Mechanisms at Play)

by

Sierra Rose McKinzie

Bachelor of Science, University of Pittsburgh, 2019

Submitted to the Graduate Faculty of the

Graduate School of Public Health in partial fulfillment

of the requirements for the degree of

Master of Science

University of Pittsburgh

2021

UNIVERSITY OF PITTSBURGH

GRADUATE SCHOOL OF PUBLIC HEALTH

This thesis was presented

by

Sierra Rose McKinzie

It was defended on

December 16, 2021

and approved by

Dr. Beth Roman, Associate Professor, Human Genetics

Dr. Francis Amrit Gandhi, Research Assistant Professor, Pediatrics

Dr. Yesim Demirci, Associate Professor, Human Genetics

Thesis Advisor: Dr. Arjumand Ghazi, Associate Professor, Pediatrics

Regulation of Lipid-Droplet Alterations Upon Infection (Molecular Mechanisms at Play)

Sierra Rose McKinzie, MS

University of Pittsburgh, 2021

The immune response is an energy intensive process. To fuel the response, organisms must effectively utilize limited resources. Consequently, fueling one physiological response can diminish resource allocation towards another. Both fertility and immunity utilize energy stores in the form of lipids to meet their energy demands. Studies in model organisms and in nature have suggested that fertility and immunity are mutually antagonistic. However, the molecular mechanisms underlying this relationship remain poorly understood. Immune response to acute pathogenic infections depends on lipid mobilization for energy. Similarly, reproduction is also highly dependent on lipid resources. Here, we have used the model organism, *Caenorhabditis elegans*, to address the role of lipid metabolism in the immunity-fertility relationship. These studies are based on the discoveries in the Ghazi lab that a transcription elongation and splicing factor, TCER-1, promotes fertility and represses immunity likely by modulating lipid-metabolic genes and processes. To understand how lipid stores are impacted by infection, wild-type worms expressing the lipid droplet resident protein PLIN-1, tagged with GFP (PLIN-1::GFP), were imaged after pathogenic exposure. These experiments revealed that pathogenic infection decreases individual lipid droplet size and total volume compared. This finding agrees with previous work and establishes this method as suitable for future studies investigating the impact of TCER-1 and infection on lipid droplets. Furthermore, we evaluated the impact of the loss of function of TCER-1-target lipases, *lipl-1* and *lipl-2*, on immune resilience. In nutrient-poor conditions, lipase-like (*lipl*) genes are a critical factor in the mobilization of lipids. However,

their role in infection response has not been studied. Preliminary data from the Ghazi lab suggests that TCER-1 represses *lipl-1* and *lipl-2* to inhibit immunity. Our experiments here showed that within the *C. elegans* immune system, both *lipl-1* and *lipl-2* are necessary for immune resilience. These findings suggest lipid metabolism is a crucial target of TCER-1 and verify a new method to investigate its effect on lipid droplet characteristics. They will contribute towards an increased understanding of the dynamics of immune responses and are of particular public health relevance as the COVID19 pandemic unfolds.

Table of Contents

List of Tables

List of Figures

Acknowledgments

I want to thank my mentor and advisor, Dr. Arjumand Ghazi, for providing me with the resources and encouragement I needed to work on this thesis project. Dr. Ghazi encouraged me to excel in my academics and research no matter the obstacles faced. I sincerely thank Dr. Ghazi for believing in me during my time in her lab.

I want to thank Dr. Francis Amrit, who consistently and cheerfully provided guidance and knowledge throughout my time in the Ghazi lab. He was a major supporter of me and allowed me to believe in myself and my own abilities.

I would like to give a special thank you to Laura Bahr of the Ghazi lab, who became an incredible friend and mentor during my thesis project. Laura worked closely with me during this thesis project, and without her, none of this could have been possible.

My heartfelt gratitude goes out to the rest of the Ghazi lab for being a kind and nurturing environment that has paved the way for my future success in the field of research science. So it was with a heavy heart, I left the lab family at the end of the semester.

Finally, I want to thank my committee members Dr. Ghazi, Dr. Amrit, Dr. Beth Roman, and Dr. Yesim Demirci, for coming together and assembling a special committee. During the COVID19 pandemic, having such a helpful and communitive group cannot be taken for granted, and I can barely begin to explain my gratitude for them.

1.0 Introduction

Physiological processes such as fertility and immunity are energetically taxing on organisms. Balancing the demands of these competing processes requires tight coordination due to a shared requirement of energetic resources [1,2]. Furthermore, fertility and immunity are thought to be mutually antagonistic, as demonstrated by the increased susceptibility to infections observed in pregnant women. In addition, when aberrant or overactive immune activity is observed in pregnant women, the body's response can be terminal to the pregnancy [3]. While fertility and immunity are inextricably linked, the underlying molecular mechanisms that tie these connections are poorly understood. Despite the lack of knowledge, it is known that lipid metabolism is an important regulator of both fertility and immune activation [4-7].

Studying physiological processes such as fertility and immunity is challenging in mammals due to their long lifespan and low fecundity. The nematode worm *Caenorhabditis elegans* has a comparatively shorter lifespan, averaging two to three weeks in normal lab conditions. *C. elegans* also have high fecundity, with an average worm laying around 300 eggs in its lifetime [8,9]. Continuously, *C. elegans* shares many biological pathways lipid metabolism and energy homeostasis with humans and is an established model organism to study lipid metabolism and storage [10-12]. The animal solely utilizes innate immunity, with its major immune pathways being highly conserved. Furthermore, the nematode worm is optically transparent; thus, lipid storage and progeny development may be observed in *vivo* [9]. These characteristics of the model organism provide simplified means to study the dynamics of lipid signaling of fertility and immunity.

The Ghazi lab investigates the mechanisms underlying maternal-fetal lipid allocation during normal health and during infections. Previously, the lab has shown that the gene *tcer-1*, which encodes the homolog of the human transcription elongation/splicing factor, TCERG1, broadly remodels lipid metabolism and promotes fertility while suppressing immune resistance. Uniquely, *tcer-1* mutants exhibit increased resistance to infections [13-16]. Thus, *tcer-1* is a great tool to study the fertility/immunity trade-off.

Fertility is an energetically demanding process relying significantly on lipid stores [17]. It is known that in *Caenorhabditis elegans*, about 90% of intestinal lipids are sent to developing embryos; however, lipids within the hypodermis remain in the maternal soma [13-16]. Therefore, tissue-specific lipid storage may indicate an energetic investment in immunity versus fertility. Triggering the immune system is interconnected to the redistribution of available energy for organisms to combat infections by prioritizing the immune response. One bioenergetic resource for this is lipid droplets [18-19].

Previously, data from the Ghazi lab showed that lipid stores in both *tcer-1(-)* and wild-type animals were reduced in the anterior intestine by infection (Bahr and Ghazi, Unpublished). Labeling stored lipids by Oil Red O (ORO) staining demonstrated that *tcer-1(-)* animals have perturbed lipid storage patterns. ORO staining of *tcer-1(-)* worms revealed a speckling of lipid droplets within the hypodermal tissues, that was not observed in wild-type worms (Bahr and Ghazi, Unpublished). The speckling pattern of the *tcer-1(-)* animals was seen in both control and infection conditions (Bahr and Ghazi, Unpublished). However, using ORO staining alone, we cannot precisely differentiate between specific tissues. Therefore, here, we utilized transgenic strains expressing the lipid droplet resident protein PLIN-1, tagged with GFP (PLIN-1::GFP) in

specific tissues, to compare lipid storage between normal worms and *tcer-1* mutants under pathogenic and normal conditions.

C. elegans' innate immunity and TCER-1 regulation converge at lipid metabolism. To identify mechanistic effectors of TCER-1, the Ghazi lab preformed an RNA-seq study comparing gene regulation by TCER-1 and infection (Amrit and Ghazi, Unpublished). The analysis of the preliminary data from the Ghazi lab show that *tcer-1* and infection antagonistically regulate *tcer-1(-)* worms have increased mRNA expression of two *lipl* lipase genes, *lipl-1* and *lipl-2 suggesting that* these genes may play roles in immunity (Amrit and Ghazi, Unpublished). In normal environments, LIPL lipases work to degrade lipids from lipid droplets through lipophagy. In germline-less *C. elegans* mutants, increased lipase activity contributes to prolonged lifespan [20]. Prior studies have shown that decreased reproduction in many organisms correlates to heightened fat storage and increased longevity. However, the impact of redistributing lipids and its relationship to lifespan extension is still not fully understood [13-16; 21-22]. To test the role of these *lipl* genes on TCER-1's function in reproduction and immunity, we have individually introduced mutants of *lipl-1* and *lipl-2* into the *tcer-1(-)* background and examined their impact on immunoresistance.

This study aimed to examine the influence of *tcer-1* and its downstream target lipases, *lipl-1* and *lipl-2*, in both lipid droplet metabolic alterations and immune resistance in response to infection by the opportunistic pathogen *Pseudomonas aeruginosa* strain PA14 (PA14). We tested the hypothesis that TCER-1 modulates immune resistance in part by remodeling lipid metabolism, through regulation of *lipl-1/2*. Furthermore, we verify a method to examine the impact of TCER-1 and infection on tissue-specific lipid storage.

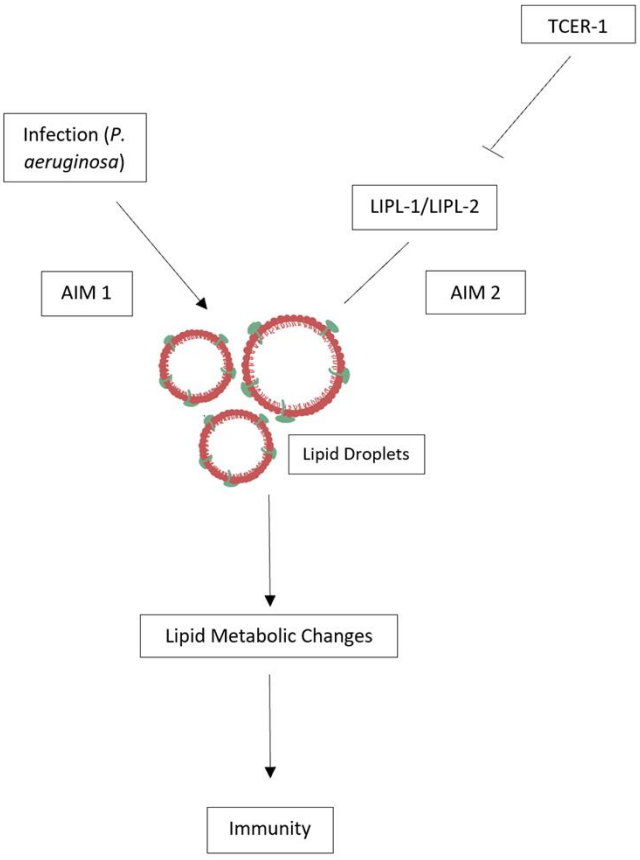

Figure 1: Graphical Abstract.

Figure 1 depicts a visulized hypothesis figure. AIM One: Understand the influence of TCER-1 on lipid droplet alterations in response to infection. AIM Two: Understand the impact of LIPL-1 and LIPL-2 on immunity in wild-type and *tcer-1(-)* genetic backgrounds.

2.0 Methods

2.1 *Caenorhabditis elegans* Strains and Culture

All strains used in this study were developed and maintained on a standard nematode growth medium (NGM) utilizing live *Escherichia. coli* strain OP50 as the food source at 15 °C as this temperature is more stable for the mutants. The *C. elegans* strains in this study include N2 (Wild type), AGP278 *tcer-1*(-)(*glm27*), XD3971 *xdIs143*[*Pdaf-22PLIN1::GFProl-6*(*su1006*)], XD2458 *xdIs56[P Y37A1B.5 PLIN1::GFP rol-6(su1006)]*, AGP314a (*glm27*; *xdIs143*[*Pdaf-22PLIN1::GFProl-6*(*su1006*)]), AGP318a (*glm27*; *xdIs56[PY37A1B.5PLIN1::GFProl-6(su1006)]*), AGP183 *lipl-1* loss of function mutant (tm1954), AGP185a *lipl-2* loss of function mutant (tm4324), AGP320a (glm27;tm1954) AGP321a (glm27; tm4324). AGP314a, AGP318a, AGP320a, and AGP321a were all created by genetic crossing (see crossing schematics below).

2.1.1 Crossing Schematics

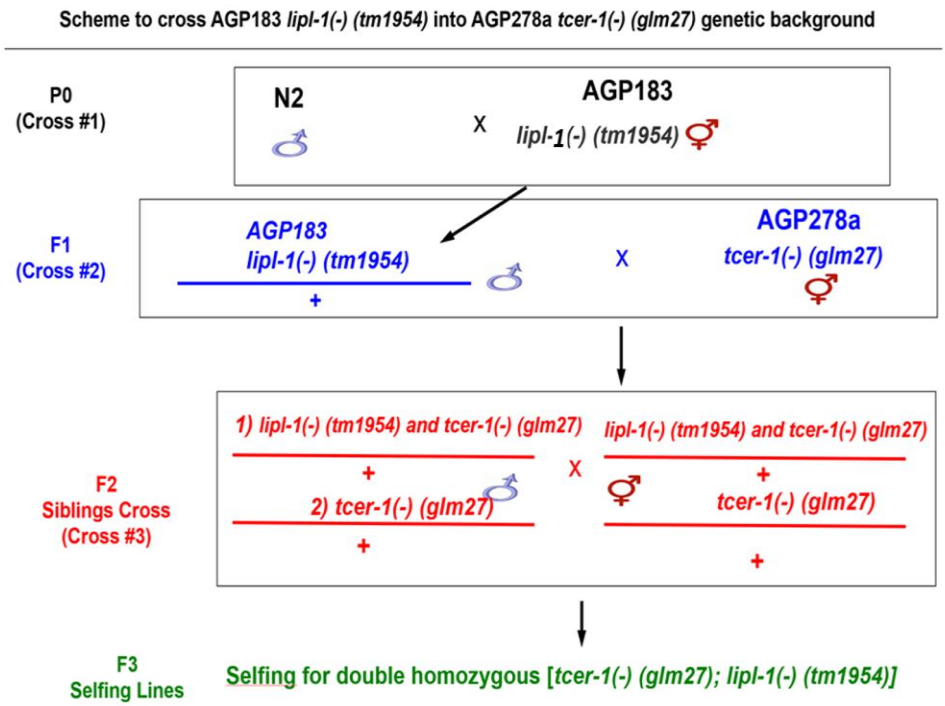

Figure 2: Crossing Scheme for AGP183 into AGP278a genetic background.

N2 represents the wild-type. After selfing, genotyping was preformed to confirm double homozygousity.

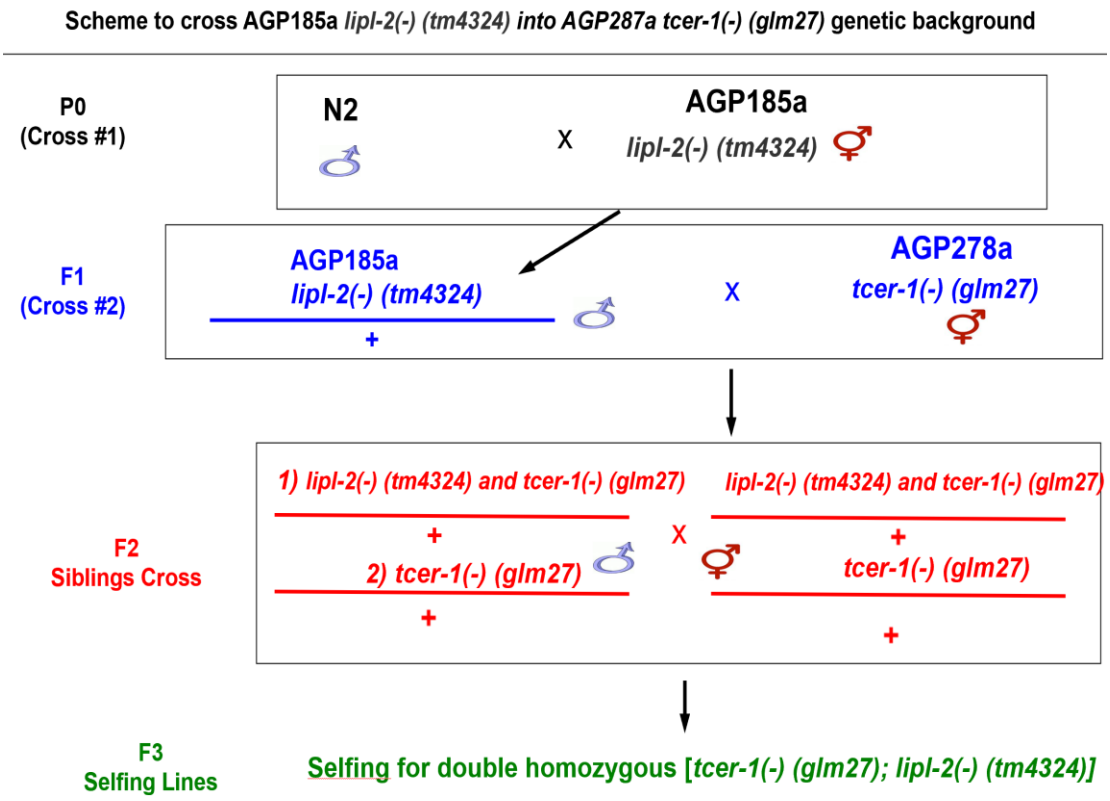

Figure 3: Crossing Schematic for AGP185a into AGP278a genetic background.

N2 represents the wild-type. After selfing, genotyping was preformed to confirm double homozygousity.

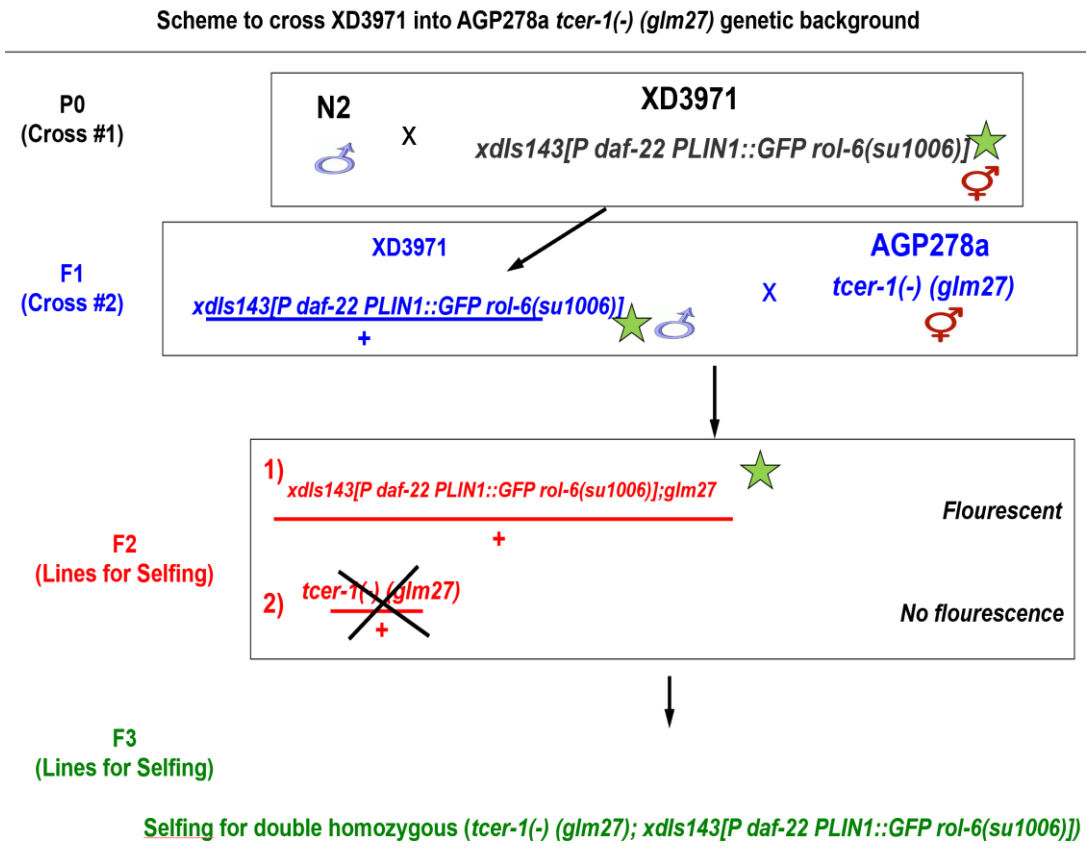

Figure 4: Crossing Schematic for XD3971 into the AGP278a genetic background.

N2 represents the wild-type. After selfing, genotyping was preformed to confirm double homozygousity.

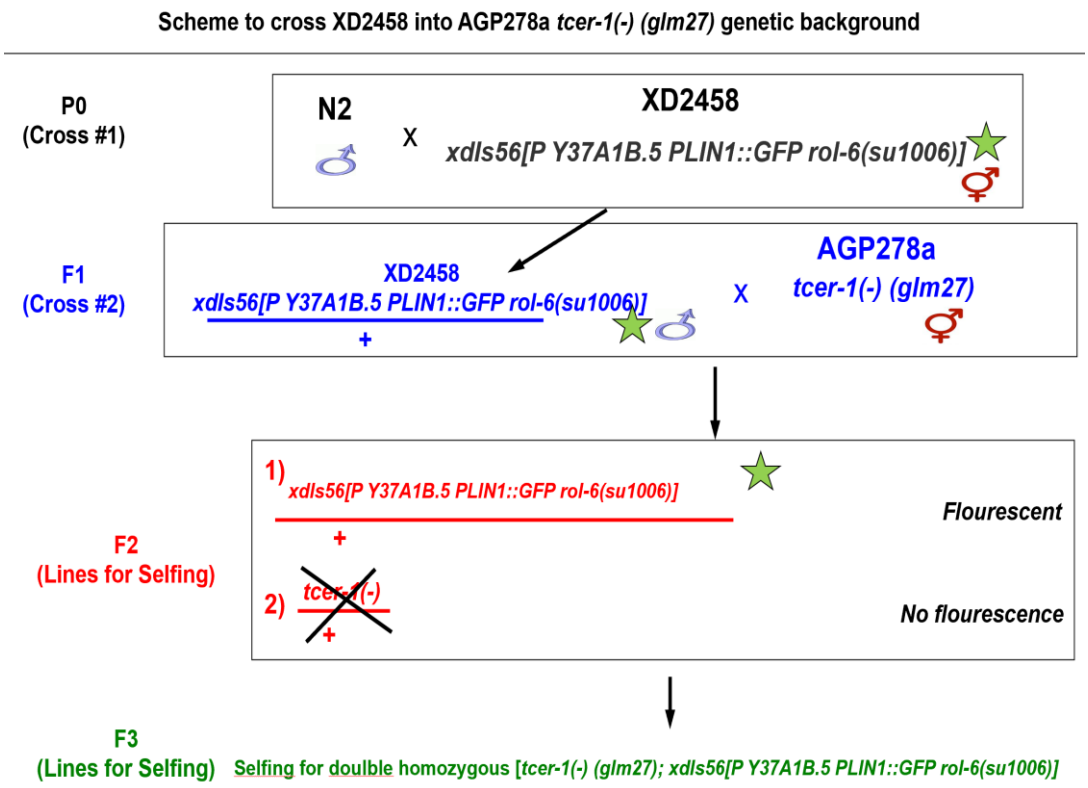

Figure 5: Crossing Schematic for XD2458 into AGP278a genetic background.

N2 represents the wild-type. After selfing, genotyping was preformed to confirm double homozygousity.

2.2 Confocal Microscopy

A Nikon Eclipse Ti A1r confocal scanning confocal microscope was used for imaging. All samples were imaged at 60x magnification with a pinhole of 1.2 (AU), gain (high voltage) of 95, and a laser power of 1.3. Three independent trials each were conducted for imaging the intestinal and hypodermal PLIN-GFP reporters in wild-type and *tcer-1(-)* backgrounds. For all trials, 10-20 worms of each strain were staged at day one and placed on PA14 pathogenic plates and OP50 NGM plates. Pathogenic plates were made using the same method as previously described (see Methods section). In addition, worms were staged as day-one animals to match the exposure time of worms in the pathogen stress assay experiments. Animals of all strains and conditions were incubated at 25 °C for 16 hours before imaging. Confocal images of Z-stacks were performed in 0.5 µm steps for 21 steps focusing on the first two anterior intestinal cells for intestinal lipid-droplets. For hypodermal reporters, images were taken from hypodermal cells adjacent to the second to fourth anterior intestinal cells**.**

2.2.1 Statistical Analysis of Confocal Imaging

A total of three trials were conducted comparing the wild-type strain XD3971xdIs143[Pdaf-22PLIN1::GFProl-6(su1006)] on normal OP50 versus PA14 infection conditions. First, 3 to 4 worms were selected for each test for imaging per condition. Then, Z-stacks were obtained by confocal microscopy and for each worm in 0.5 µm steps for a total of 21 steps. Of the 9-12 total worms, 3-4 worms were then selected for each condition for image analysis. To analyze images, every fourth slice of each Z-stack was chosen to be analyzed, totaling six slices per worm. The selected slices were then transported into the ImageJ software

system (ImageJ (nih.gov)). A novel analysis method was implemented using ImageJ software to manually measure the amount and size of individual lipid droplets (LDs). To make faint LDs easier to identify, images were altered to have enhanced contrast through the software. The perimeter was measured of each LD by tracing the LD. Then, the data was transferred to a Microsoft Excel spreadsheet. Using the perimeter, diameter and volume were calculated and graphed on GraphPad Prism software.

2.3 Pathogenic Stress Assays

An established model of infection, *Pseudomonas aeruginosa* (strain PA14), was utilized in this study [23,24]. The strain was streaked from frozen stocks onto high-peptone plates (NGM plates modified to contain 0.35% peptone instead of 0.25%), incubated at 37 °C overnight, and stored at 4 °C to make the streak plate. Each streak plate was kept for a maximum time of one week before creating a fresh plate. From the streak plate, single colonies were inoculated and grown in King's broth at 37 °C with overnight shaking. Next, 20 µl of this broth culture were seeded onto slow killing (SK) high-peptone plates and incubated for 24 hours at 37 °C. Before use, plates were left for at least 24 hours, but no more than 48 hours, at room temperature. When worms are exposed to pathogens, many deaths are caused by eggs hatching internally of the mother, often referred to as bagging. To ensure an accurate interpretation of assay results and minimize censoring, all tested worm lines were treated with 100 µg per ml of 5'-fluorodeoxyuridine (FUdR). FUdR is used to cause the production of non-viable embryos, thus avoiding internal hatching. Worms were treated with FUdR on NGM plates with OP50. *C. elegans* were exposed to FUdR for 24 h at 15 °C before transferring to PA14 SK plates. 20 to 40

day-1 staged worms were moved to pathogenic plates per condition for each trial. Each condition consisted of 3-5 plates, totaling 100-125 worms. The plates were maintained at 25 °C and monitored for survival at 0, 24, 42, 48, 54, 66, 72, 78, 90, 96, 102, 114, 120, 126, 138-hour marks or until all animals were dead. Every 24 hours, the remaining worms were transferred to fresh PA14 seeded plates to prevent excesses spreading of the PA14 lawn.

2.3.1 Statistical Analysis of Pathogen Stress Assay Data

In this research, all data are expressed as mean (m) ± standard error of the mean (SEM) unless otherwise noted. Graphs from pathogenic stress assays were plotted using the Kaplan Meier Survival test on OASIS2 2 (https://sbi.postech. ac.kr/oasis2/) [25]. OASIS2 program was also used to analyze the statistical significance and restricted mean data, where statistically significant results have a p-value of 0.05 or below. Three experimental trials were performed, testing 100-125 worms per condition per trial in the method previously described in the methods.

3.0 Results

3.1 Lipid Droplet Size and Content are Decreased After Infection

To understand the influence of *tcer-1* mutation on lipid droplet alterations in response to infection we aimed to visualize what happens to lipid droplets within specific tissues and upon infection. Transgenic strains expressing the lipid droplet resident protein PLIN-1, tagged to GFP (PLIN-1::GFP) were compared under *E. coli* OP50 (control) or *P. aeruginosa* PA14 (infection) conditions. First, day one worms were transferred to either control or infection plates, they were then incubated at 25^{o}C for 16 hours. After exposure, confocal imaging was performed as described in the methods section.

Due to the novelty of measuring individual lipid droplets within tissue specific regions of the worm, the Ghazi lab was faced with devising a new method of analysis. A member of the Ghazi lab, Laura Bahr, devised a method to manually measure lipid droplets using the ImageJ software. The details of this analysis protocol are described in the methods section.

Here, the analysis of confocal imaging focuses on wild-type intestinal reporters. We use the wild-type strain to serve as a control to validate the integrity of the novel analysis method. As seen in Figure 6, a clear visual shows that wild-type worms have reduced amount of lipid droplets within the intestine after pathogenic exposure. To verify what was observed visually, the perimeter measurements of individual lipid droplets were collected using ImageJ. Results of these confocal imaging experiments suggest that lipid droplet size and volume is reduced in response to infection similar to what has been observed by Laura Bahr using ORO staining (Figure 7, Bahr and Ghazi, Unpublished).

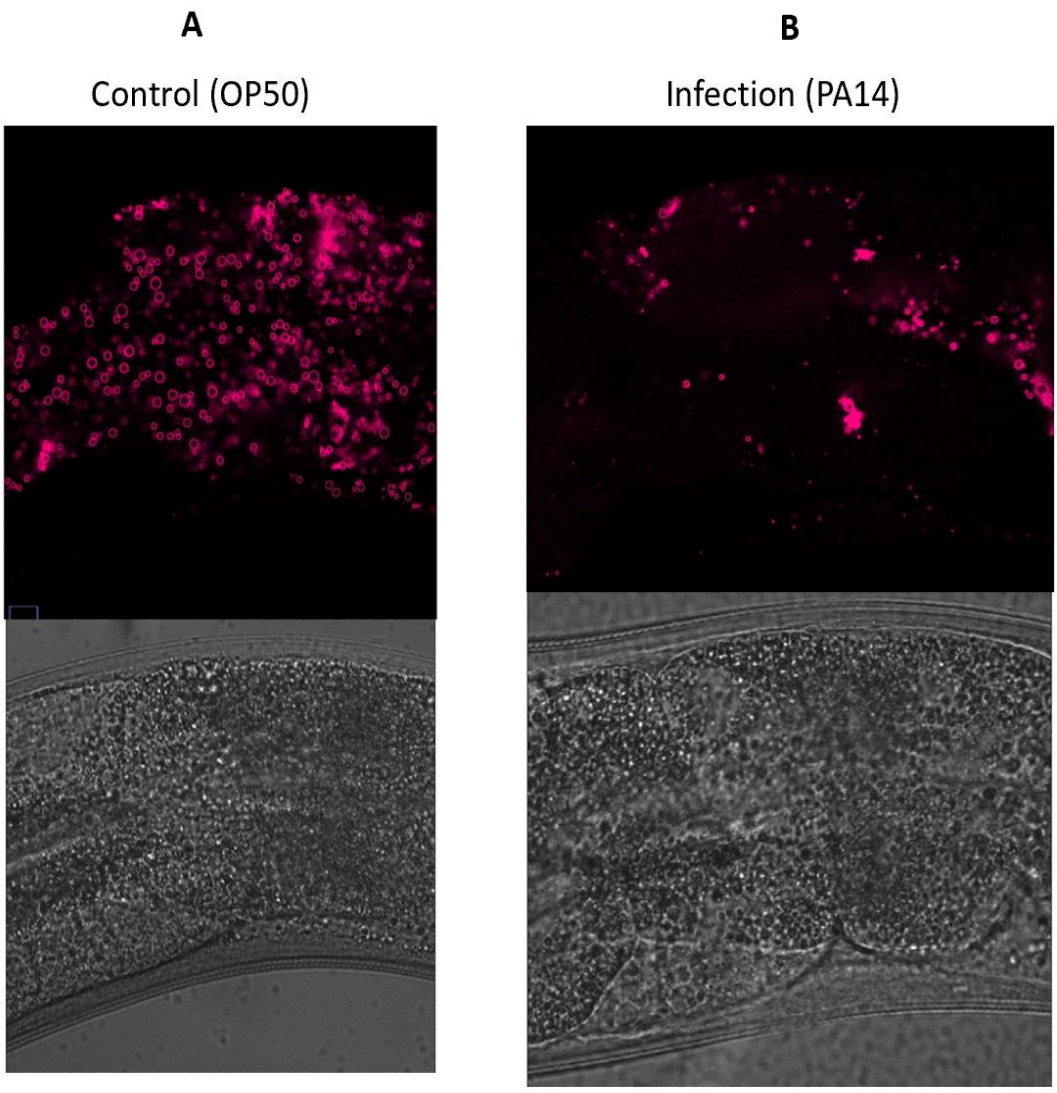

Figure 6: Intestinal Confocal Imaging of Lipid Droplets in WT *C. elegans* on *E. coli* (OP50) and *P. aeruginosa* (PA14).

Confocal images of Z-stacks were taken of the first two anterior intestinal cells. Images were altered to show enhanced contrast to more clearly visualize lipid droplets (LDs).. Individual LDs were traced to measure perimeter. Further details on how these images were obtained and analyzed are noted in the methods section. Three trials were conducted with 3-4 worms of each strain being imaged per condition, per trial. Total data from all image analyses were run and graphed using the GraphPad Prism software (See figure 3).

(A) Wild-type strain XD3971xdIs143[Pdaf-22PLIN1::GFProl-6(su1006)] *C. elegans* on *E. coli* (OP50) with brightfield image included for scale.

(B) Wild-type strain XD3971xdIs143[Pdaf-22PLIN1::GFProl-6(su1006)] *C. elegans* on *P. aeruginosa* (PA14) with brightfield image included for scale

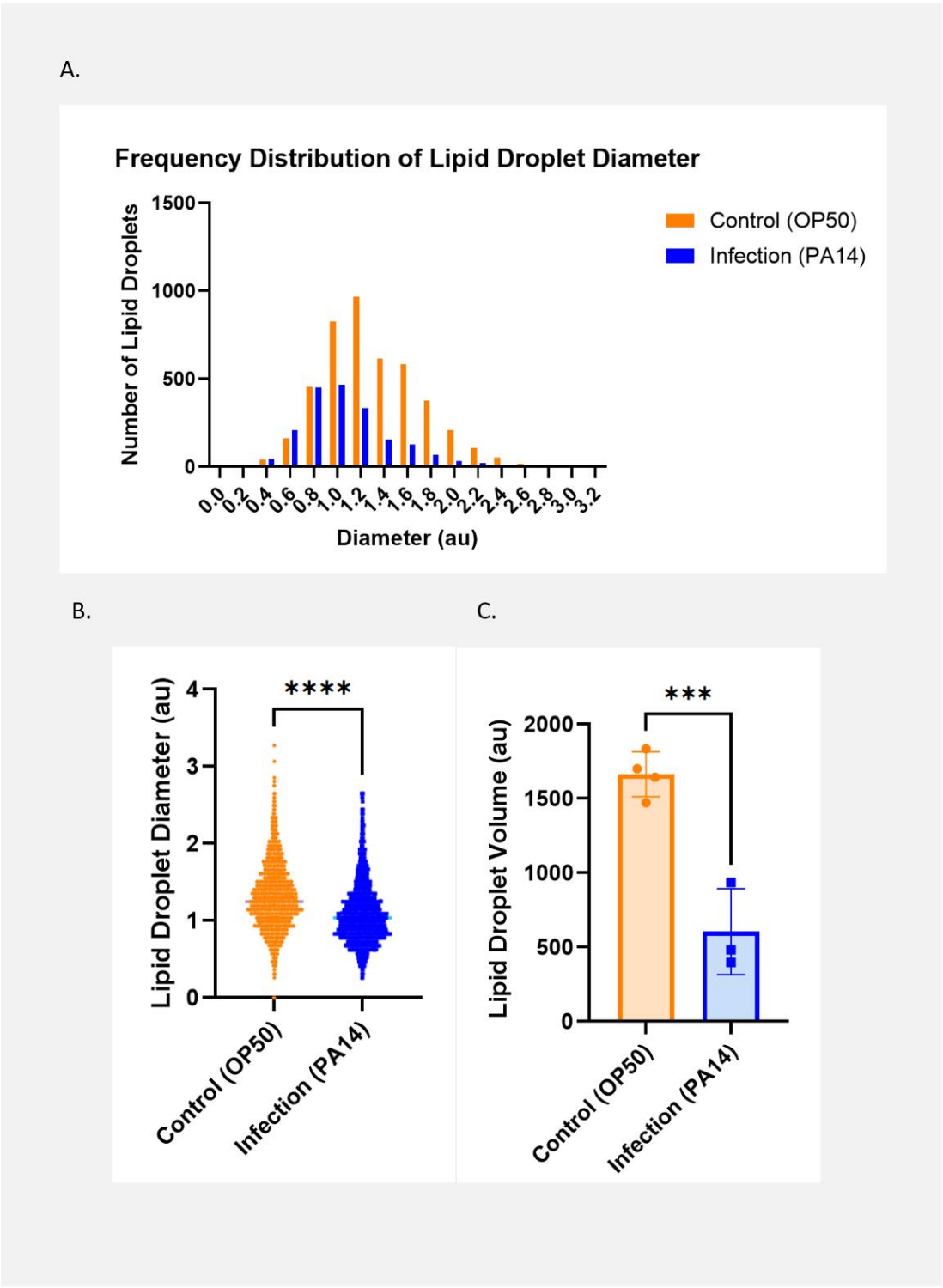

Figure 7: Lipid Droplet Size and Volume is Reduced in Response to Infection.

Figure 8 presents the statistical analysis of confocal images from three trials. For each trial, 3-4 worms were imaged per condition. Of the 9-12 total worms, 3-4 worms were then selected for image analysis per

conditon. After collecting perimeter measurements, diameter and volume were calculated. (A) Histogram measuring the frequency distribution of lipid droplet diameter in arbitrary units (au). (B) Scatter plot comparing lipid droplet diameters between control and infection conditions. (C) Scatter plot with bar comparing volumes of control and infection conditions. The orange refers to the control group, and the blue indicates the infection group. Asterisks indicate statistical significance <0.05 (*), <0.01 (**), <0.001 (***) and <0.0001 (****). Statistical significance was defined by using an unpaired one-tailed t-test. All graphs were generated using the software GraphPad Prism.

3.2 LIPL Lipases Are Essential in Combating Acute Pathogenic Infections

To understand the role of LIPL-1 and LIPL-2 in *C. elegans* immune response, survival of animals with loss of function mutations in each of the genes were compared in both wild-type and *tcer-1(-)* genetic backgrounds upon exposure to the pathogen *P. aeruginosa* (strain PA14). After treatment of FUdR of staged L4 *C. elegans*, Day one adults were transferred to plates seeded with PA14, incubated at 25ºC, and monitored for survival until all animals were deceased or censored. Animals were counted dead if they failed to respond to the gentle prodding of the head. As shown in Figure 8, both *lipl-1(-)* and *lipl-2(-)* mutants show decreased survival in the presence of pathogen compared to wild-type animals, and both mutations shortened the survival of *tcer-1* mutants on PA14 as well (Figure 8 A-C). Thus, these results suggest that *lipl-1* and *lipl-2* are necessary for optimal immune resilience in response to acute pathogenic exposure in normal animals and they contribute to the enhanced immunoresistance of *tcer-1* mutants.

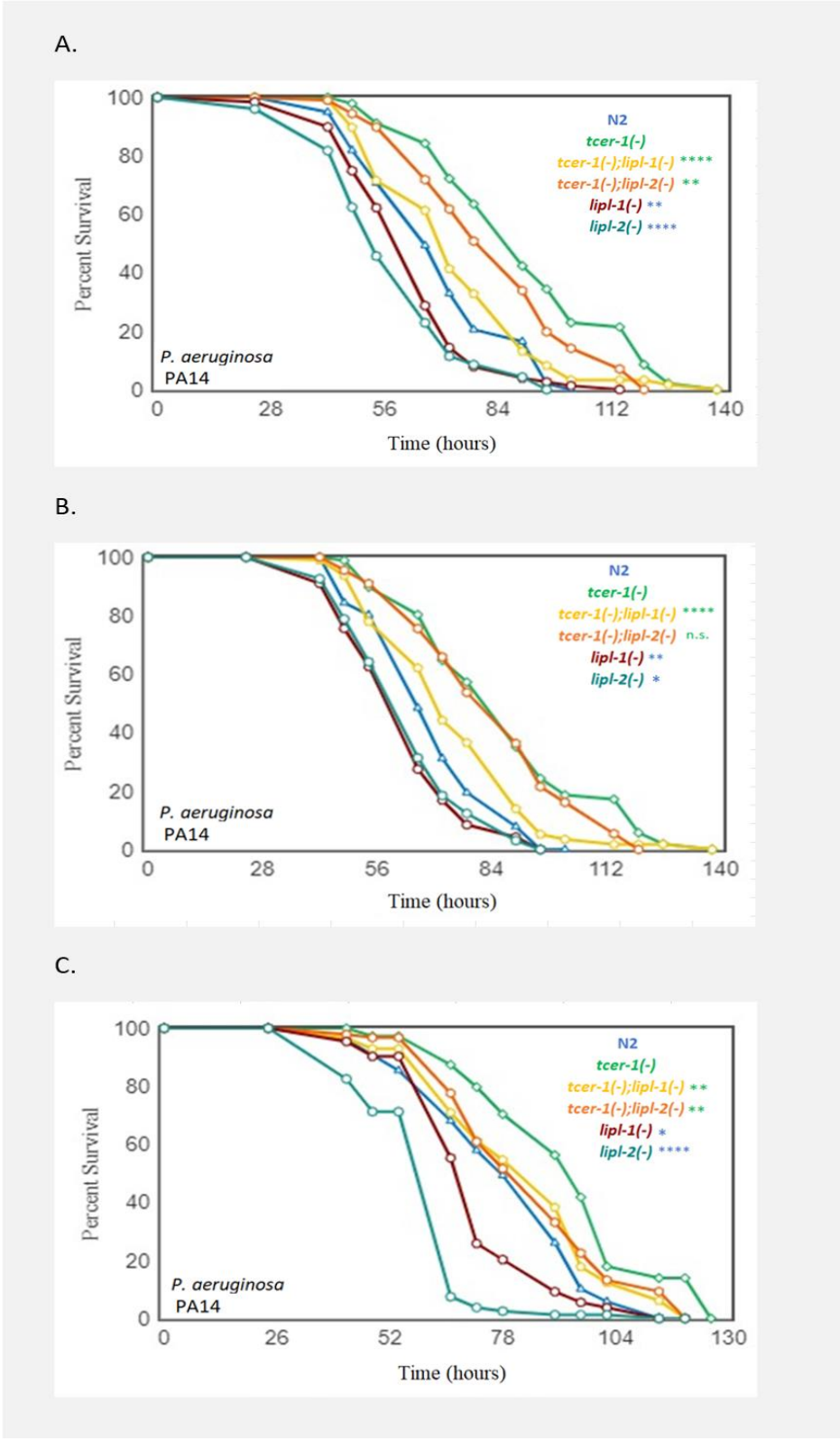

Figure 8: LIPL-1/2 loss of function suppress immunoresistance in N2 (Wild-Type) and *tcer-1(-) C. elegans*.

Survival of day 1 staged, wild-type *C. elegans* (N2, blue), *tcer-1(-)* (green), *tcer-1(-);lipl-1(-)* (yellow), *tcer-1(-);lipl-2(-)* (orange), *lipl-1(-)* (maroon), and *lipl-2(-)* (turquoise) worms exposed to acute pathogenic infection, using *P. aeruginosa*, on slow killing (SK) plates. (A) trial one, n=125 (B) trial two n=125. (C) trial three n=100. Survival data was analyzed on OASIS2 software using the Kaplan−Meier test. Asterisks indicate statistical significance <0.05 (*), <0.01 (**), <0.001 (***) and <0.0001 (****). Asterisks are color-coded to indicate strains of comparison. The mean lifespan data is shown Table 1.

Table 1: Restricted Mean Data for Pathogen Assay Trials

Trial One	No. of Subjects Observed	Mean (hours)	Standard Error
N2	62	69.59	1.99
tcer-1(-)	73	91.21	2.44
tcer-1(-);lipl-1(-)	75	74.26	2.17
tcer-1(-);lipl-2(-)	76	83.82	2.21
lipl-1(-)	84	63.13	1.62
lipl-2(-)	88	58.75	1.63

Trial Two	No. of Subjects Observed	Mean (hours)	Standard Error
N2	49	70.28	1.92
tcer-1(-)	75	87.69	2.39
tcer-1(-);lipl-1(-)	72	75.66	2.05
tcer-1(-);lipl-2(-)	78	85.31	2.14
lipl-1(-)	66	63.44	1.63
lipl-2(-)	65	64.63	1.65

Trial Three	No. of Subjects Observed	Mean (hours)	Standard Error
N2	71	79.80	2.15
tcer-1(-)	55	93.68	2.42
tcer-1(-);lipl-1(-)	76	84.20	2.18
tcer-1(-);lipl-2(-)	55	85.27	2.04
lipl-1(-)	55	72.59	1.98
lipl-2(-)	80	61.05	1.38

4.0 Discussion

The immune response and metabolic reprogramming of lipids are interconnected [26-29]. However, despite reports of the dynamic morphologies and adaptations of lipid droplets in *in-vivo* studies, their alteration to infectious conditions is understudied [26]. In addition, lipid mobilization, which is crucial in pathogen resistance, can be attributed to LIPL lipases, but their specific roles in infection have yet to be studied until now. Here we found that, within the intestine of *C. elegans*, lipid droplets change in response to pathogenic exposure. Data from confocal imaging revealed that wild-type *C. elegans* had reduced lipid droplet content and size when exposed to pathogenic conditions. Due to the study's novelty, the lab was faced with devising a way to correctly measure the changes of lipid droplets between the control and infection conditions (see Methods). Initially, the experimental goal was to understand the influence of *tcer-1(-)* on lipid droplet alterations in response to infection. However, the wild-type intestinal reporter strain was first tested on both control and infection conditions to validate the method. After analyzing the data of this experiment, the results were consistent with the preliminary ORO data from the Ghazi lab. Thus, the novel method was validated.

As shown in Figure 9 (Supplementary Materials section), the intestinal reporter shows a partial decrease in lipid droplet in *tcer-1(-)* mutants, but not to the extent observed in their wild-type counterparts. This could potentially indicate that *tcer-1(-)* animals retain more lipid droplets than wild-type worms when exposed to infection. Sup. Figure 10 shows the wild-type hypodermal tissue-specific reporters on control and infection conditions. Once again, a visual decrease in lipid droplets is observed. Comparatively, this decrease is modest in *tcer-1(-)* mutants as seen in Figure 11. Our preliminary analyses indicated that, in addition to number of

droplets, the total volume of lipid droplets decreases when the animals are exposed to infection. Further quantitative analysis of the images acquired during this study will test the validity of these visual trends.

During image analysis, we found lipid droplets existed in different states. In both experimental conditions, clear, brightly pigmented, ring-like lipid droplet structures accounted for the majority of labeled lipids. A minor fraction had lipid droplets that were faint and hard to measure, potentially leading to under-sampling. Similarly, in some locations the many droplets appeared together to form 'clusters', to the degree that multiple or all lipid droplet borders were indistinguishable from one another. This may also potentially produce under-sampling of lipids within the cluster and potential variability in diameter measurements if the boundaries of the lipid droplet are accurately determined. Therefore, only clearly defined LDs were selected when sampling within a cluster. Moreover, in primarily the pathogenic condition, solid-core structures were observed. However, unlike the ring-shaped lipid droplets with a defined lumen, these structures appeared opaque spherical bodies. Therefore, these structures were excluded from analyses to avoid misrepresenting the data. Similar trends of lipid droplet alterations were also observed in the unanalyzed trials shown in Figures 9-11. Overall, when worms were exposed to infection, both decreased lipid droplets and increased clustering and solid core bodies were seen. While the analysis method has limitations, it remains a valid technique to measure lipid droplets.

Data from the pathogen stress assays suggest that LIPL-1/2 loss of function suppresses Immune resistance. Here, we see that in three out of three trials, both *lipl-1(-)* and *lipl-2(-)* animals show decreased pathogen resistance in the wild-type background (Figure A-C). Similarly, *tcer-1(-);lipl-1(-)* animals consistently displayed significant decreases in survivability to infection compared to *tcer-1(-)* alone. Lastly, *tcer-1(-);lipl-2(-)* worms had substantial declines

in two out of three trials in comparison to *tcer-1(-)* animals, whereas in the second trial, there was no significant difference between the two groups (p-value of 0.22).

Within the pathogen stress assay experiments, the animals were treated with FUdR. This treatment is standard in experiments with *C. elegans* to render their embryos non-viable, thus preventing deaths from internal hatching, a common consequence of pathogenic exposure [30]. However, FUdR has been attributed to affecting stress resistance and varying lifespan, meaning that results taken from these assays should be interpreted with caution [31,32]**.** Still, the results gathered from this study support the claim that *lipl-1* and *lipl-2* are necessary for optimal immune resilience in response to acute pathogenic exposure (Figure 1). One possible reason why *lipl-1/2* would contribute to these results is the characteristic of lipases to release free fatty acids by hydrolyzing triglycerides, which could aid in providing the animal energy to fight off infections [33,34].

5.0 Conclusion

During the current public health crisis of the COVID19 pandemic there has been an understandable increased attention on the immune system. Therefore, it is imperative to understand the underlying molecular mechanisms that are involved in the immune response.

Our data suggests that lipid droplets are altered after pathogenic exposure in the *C. elegans'* intestine. The data also suggests that *lipl-1* and *lipl-2* lipase encoding genes are necessary for optimal immune resilience in response to acute pathogenic exposure. Together, these observations raise the possibility that lipid-metabolic pathways are integral to the molecular mechanisms underlying the immune response in *C. elegans*. Based on the data acquired in this study, the Ghazi lab has devised and validated a method for measuring and analyzing individual lipid droplets from confocal imaging of the worm body. In the future, the lab will utilize this method to further interrogate the impact of TCER-1 on lipid droplets in the intestine and hypodermis during infection. Continued studies of this topic will enhance the understanding of the molecular mechanisms that connect lipid metabolism and immune response.

Supplementary Materials

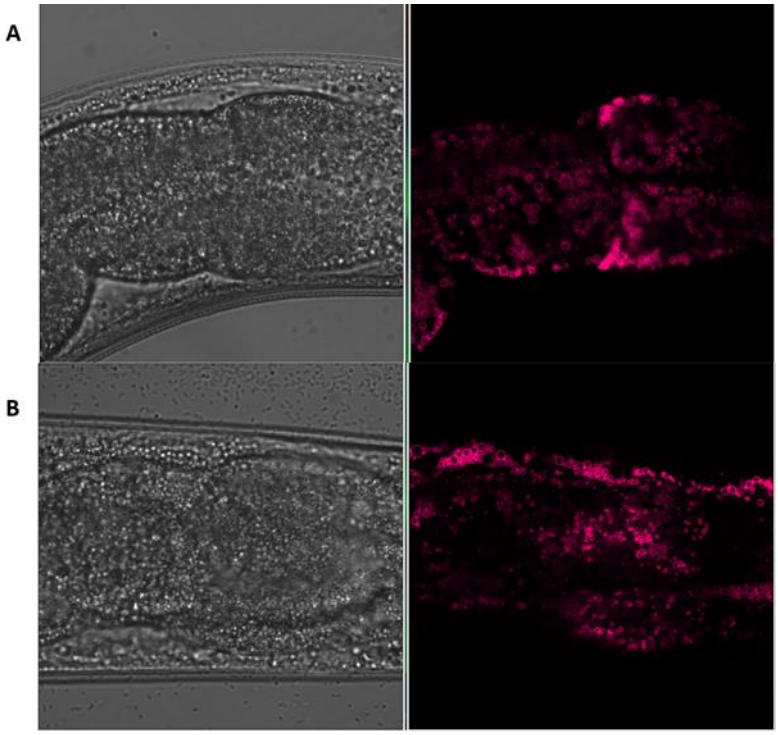

Figure 9: Intestinal Confocal Imaging of Lipid Droplets in *tcer-1(-) C. elegans* on control (OP50) and infection (PA14).

Confocal images of Z-stacks were taken of the first two anterior intestinal cells. Images were altered to show enhanced contrast to more clearly visualize lipid droplets (LDs).

(A) Intestinal reporter strain AGP314a (*glm27*; *xdIs143*[*Pdaf-22PLIN1::GFProl-6*(*su1006*)])*C. elegans* on *E. coli* (OP50) with brightfield image included for scale.

(B) Intestinal reporter strain AGP314a (*glm27*; *xdIs143*[*Pdaf-22PLIN1::GFProl-6*(*su1006*)]) *C. elegans* on *P. aeruginosa* (PA14) with brightfield image included for scale.

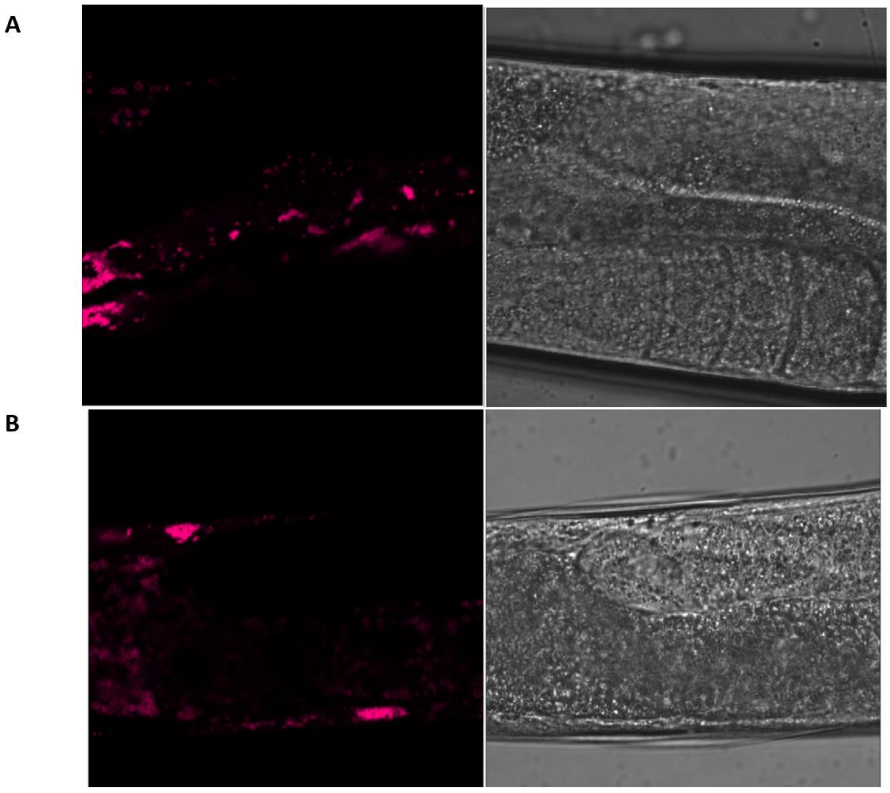

Figure 10: Hypodermal Confocal Imaging of Lipid Droplets in WT *C. elegans* on *E. coli* (OP50) and *P. aeruginosa* (PA14).

Confocal images of Z-stacks were taken of the first two anterior intestinal cells. Images were altered to show enhanced contrast to more clearly visualize lipid droplets (LDs).

(A) Wild-type hypodermal reporter strain XD2458 *xdIs56[P Y37A1B.5 PLIN1::GFP rol-6(su1006)], C. elegans* on *E. coli* (OP50) with brightfield image included for scale.

(B) Wild-type hypodermal reporter strain XD2458 *xdIs56[P Y37A1B.5 PLIN1::GFP rol-6(su1006)], C. elegans* on *P. aeruginosa* (PA14) with brightfield image included for scale.

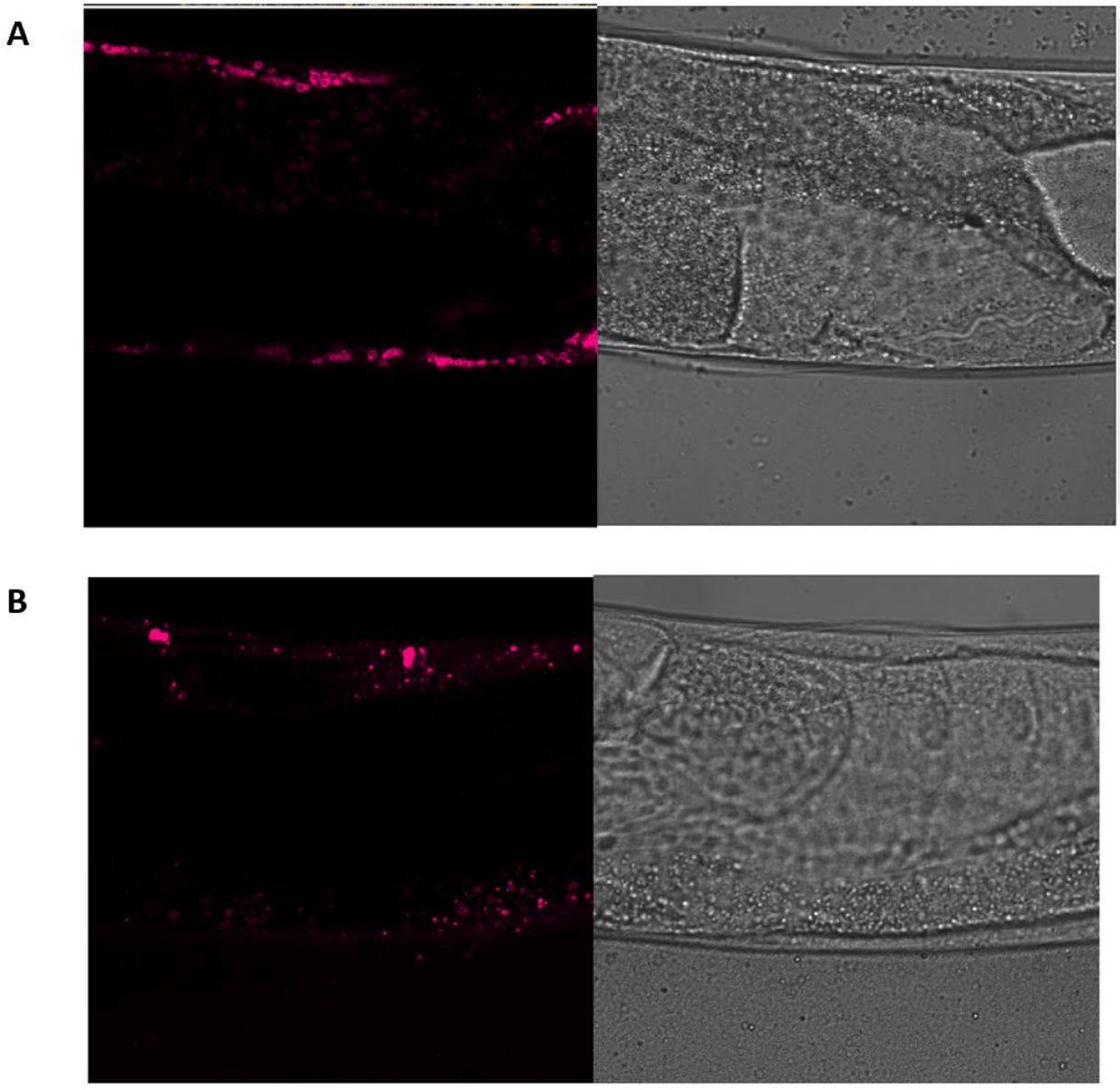

Figure 11: Hypodermal Confocal Imaging of Lipid Droplets in *tcer-1(-) C. elegans* on *E. coli* (OP50) and *P. aeruginosa* (PA14).

Confocal images of Z-stacks were taken of the first two anterior intestinal cells. Images were altered to show enhanced contrast to more clearly visualize lipid droplets (LDs).

(A) Hypodermal reporter strain AGP318a (*glm27*; *xdIs56[PY37A1B.5PLIN1::GFProl-6(su1006)]*), *C. elegans* on *E. coli* (OP50) with brightfield image included for scale.

(B) Hypodermal reporter strain AGP318a (*glm27*; *xdIs56[PY37A1B.5PLIN1::GFProl-6(su1006)]*), *C. elegans* on *P. aeruginosa* (PA14) with brightfield image included for scale.

Bibliography

1. Camille Bonneaud, et al., Assessing the Cost of Mounting an Immune Response. The American Naturalist, 2003. 161(3): p. 367-379.
2. Cox, R.M., et al., Experimental evidence for physiological costs underlying the trade-off between reproduction and survival. Functional Ecology, 2010. 24(6): p. 1262-1269.
3. Kwak-Kim, J., et al., Immunological Modes of Pregnancy Loss: Inflammation, Immune Effectors, and Stress. American Journal of Reproductive Immunology, 2014. 72(2): p. 129-140.
4. Malik, N., et al., Leptin requirement for conception, implantation, and gestation in the mouse. Endocrinology, 2001. 142(12): p. 5198-5202.
5. Michalek, R.D., et al., Cutting edge: distinct glycolytic and lipid oxidative metabolic programs are essential for effector and regulatory CD4+ T cell subsets. The Journal of Immunology, 2011. 186(6): p. 3299-3303.
6. Gerriets, V.A., et al., Metabolic programming and PDHK1 control CD4+ T cell subsets and inflammation. The Journal of clinical investigation, 2015. 125(1): p. 194-207.
7. Hubler, M.J. and A.J. Kennedy, Role of lipids in the metabolism and activation of immune cells. The Journal of nutritional biochemistry, 2016. 34: p. 1-7.
8. Lee, K.A., Linking immune defenses and life history at the levels of the individual and the species. Integrative and comparative biology, 2006. 46(6): p. 1000-1015.
9. Corsi, A.K., B. Wightman, and M. Chalfie, A transparent window into biology: a primer on Caenorhabditis elegans. Genetics, 2015. 200(2): p. 387-407.

10. Connor, A.J. and J.L. Watts, Omega-3 and Omega-6 Fatty Acid Metabolism: Modeling Growth and Disease Using Caenorhabditis elegans, in Omega Fatty Acids in Brain and Neurological Health. 2019, Elsevier. p. 107-116.
11. Srinivasan, S., Regulation of body fat in Caenorhabditis elegans. Annual review of physiology, 2015. 77: p. 161- 178.
12. Watts, J.L. and M. Ristow, Lipid and carbohydrate metabolism in Caenorhabditis elegans. Genetics, 2017. 207(2): p. 413-446.
13. Ghazi, A., Henis-Korenblit, S., & Kenyon, C. (2009). A transcription elongation factor that links signals from the reproductive system to lifespan extension in Caenorhabditis elegans. PLoS Genet, 5(9), e1000639. doi:10.1371/journal.pgen.1000639
14. Seah, N. E., de Magalhaes Filho, C. D., Petrashen, A. P., Henderson, H. R., Laguer, J., Gonzalez, J., Lapierre, L. R. (2016). Autophagy-mediated longevity is modulated by lipoprotein biogenesis. Autophagy, 12(2), 261-272. doi:10.1080/15548627.2015.1127464
15. Amrit, F.R.G., et al., The longevity-promoting factor, TCER-1, widely represses stress resistance and innate immunity. Nature Communications, 2019. 10(1): p. 3042.
16. Amrit, F.R.G., et al., DAF-16 and TCER-1 facilitate adaptation to germline loss by restoring lipid homeostasis and repressing reproductive physiology in C. elegans. PLoS genetics, 2016. 12(2): p. e1005788.
17. Green, B. B., Weiss, N. S., & Daling, J. R. (1988). Risk of ovulatory infertility in relation to body weight. Fertil Steril, 50(5), 721-726.
18. Hinson, E. R., & Cresswell, P. (2009). The antiviral protein, viperin, localizes to lipid droplets via its N-terminal amphipathic alpha-helix. Proc Natl Acad Sci U S A, 106(48), 20452-20457. doi:10.1073/pnas.0911679106

19. Anand, P., S. Cermelli, Z. Li, A. Kassan, M. Bosch, R. Sigua, L. Huang, A. J. Ouellette, A. Pol, M. A. Welte, and S. P. Gross. 2012. A novel role for lipid droplets in the organismal antibacterial response. eLife. 1: e00003.
20. Ackerman, Daniel, and David Gems. "The mystery of C. elegans aging: an emerging role for fat. Distant parallels between C. elegans aging and metabolic syndrome?." BioEssays : news and reviews in molecular, cellular and developmental biology vol. 34,6 (2012): 466-71. doi:10.1002/bies.201100189
21. O'Rourke, Eyleen J, and Gary Ruvkun. "MXL-3 and HLH-30 transcriptionally link lipolysis and autophagy to nutrient availability." Nature cell biology vol. 15,6 (2013): 668-76. doi:10.1038/ncb2741
22. Hansen, Malene et al. "Reproduction, fat metabolism, and life span: what is the connection?." Cell metabolism vol. 17,1 (2013): 10-9. doi:10.1016/j.cmet.2012.12.003
23. Powell, J. R. & Ausubel, F. M. Models of Caenorhabditis elegans infection by bacterial and fungal pathogens. Methods Mol. Biol. 415, 403–427 (2008).
24. Sifri, C. D., Begun, J., Ausubel, F. M. & Calderwood, S. B. Caenorhabditis elegans as a model host for Staphylococcus aureus pathogenesis. Infect. Immun. 71, 2208–2217 (2003).
25. Han, S. K. et al. OASIS 2: online application for survival analysis 2 with features for the analysis of maximal lifespan and healthspan in aging research. Oncotarget 7, 56147–56152 (2016).
26. Wang, L., Lin, J., Yu, J., Yang, K., Sun, L., Tang, H., & Pan, L. (2021). Downregulation of Perilipin1 by the Immune Deficiency Pathway Leads to Lipid Droplet Reconfiguration

and Adaptation to Bacterial Infection in Drosophila. J Immunol, 207(9), 2347-2358. doi:10.4049/jimmunol.2100343

27. Buck, M. D., Sowell, R. T., Kaech, S. M., & Pearce, E. L. (2017). Metabolic Instruction of Immunity. Cell, 169(4), 570-586. doi:10.1016/j.cell.2017.04.004
28. Hotamisligil, G. S. (2017). Foundations of Immunometabolism and Implications for Metabolic Health and Disease. Immunity, 47(3), 406-420. doi:10.1016/j.immuni.2017.08.009
29. O'Neill, L. A., Kishton, R. J., & Rathmell, J. (2016). A guide to immunometabolism for immunologists. Nat Rev Immunol, 16(9), 553-565. doi:10.1038/nri.2016.70
30. Mitchell, D. H., Stiles, J. W., Santelli, J., & Sanadi, D. R. (1979). Synchronous growth and aging of Caenorhabditis elegans in the presence of fluorodeoxyuridine. J Gerontol, 34(1), 28-36. doi:10.1093/geronj/34.1.28
31. Angeli, S., Klang, I., Sivapatham, R., Mark, K., Zucker, D., Bhaumik, D., et al. (2013). A DNA synthesis inhibitor is protective against proteotoxic stressors via modulation of fertility pathways in Caenorhabditis elegans. Aging (Albany NY), 5(10), 759-769. doi:10.18632/aging.100605
32. Van Raamsdonk, J. M., & Hekimi, S. (2011). FUdR causes a twofold increase in the lifespan of the mitochondrial mutant gas-1. Mech Ageing Dev, 132(10), 519-521. doi:10.1016/j.mad.2011.08.006
33. Ouimet, M., Franklin, V., Mak, E., Liao, X., Tabas, I., & Marcel, Y. L. (2011). Autophagy regulates cholesterol efflux from macrophage foam cells via lysosomal acid lipase. Cell Metab, 13(6), 655-667. doi:10.1016/j.cmet.2011.03.023

34. Singh, R., Kaushik, S., Wang, Y., Xiang, Y., Novak, I., Komatsu, M., et al. (2009). Autophagy regulates lipid metabolism. Nature, 458(7242), 1131-1135. doi:10.1038/nature07976